Geometry and Electronic Structure of $CuCl_6^{4-}$ Polyhedra Doped into (3-Chloroanilinium)$_8$[$CdCl_6$]Cl_4—An EPR and Structural Investigation

Burkhard Wagner,[†] Salam A. Warda,[†] Michael A. Hitchman,*[,‡] and Dirk Reinen*[,†]

Fachbereich Chemie und Zentrum für Materialwissenschaften, Hans-Meerwein-Strasse, 35043 Marburg, Germany, and Department of Chemistry, University of Tasmania, GPO Box 252C, Hobart, Tasmania, Australia

Received November 2, 1995[⊗]

The EPR single-crystal and powder spectra of mixed crystals of (3-chloroanilinium)$_8$($Cd_{1-x}Cu_xCl_6$)Cl_4 are measured as a function of temperature and x and analyzed with respect to the geometry and bonding properties of the $CuCl_6$ polyhedra. These undergo strong distortions due to vibronic Jahn−Teller coupling, with the resulting tetragonal elongation being superimposed by a considerable orthorhombic symmetry component induced by a host site strain acting as a compression along the crystallographic a axis. This strain becomes apparent in the cadmium compound ($x = 0$), whose crystal structure is also reported [$a = 8.701(2)$ Å, $b = 13.975(2)$ Å, $c = 14.173(2)$ Å, $\alpha = 81.62(1)°$, $\beta = 72.92(1)°$, $\gamma = 77.57(1)°$, triclinic $P\bar{1}$, $Z = 1$]. A calculation of the ground state potential surface and its vibronic structure nicely reproduces the g values, Cu−Cl spacings, and ligand field data. At high copper concentrations (including $x = 1$), the $CuCl_6$ polyhedra are coupled elastically, with the long axes of neighboring polyhedra having perpendicular orientations. The elastic correlation presumably is not of the long-range antiferrodistortive type, however. Above about 55 K, the angular Jahn−Teller distortion component becomes dynamically averaged within the time scale of the EPR experiment, leading to local tetragonally compressed $CuCl_6$ octahedra.

Introduction

A previous crystal structure determination of (3-Cl-an)$_8$-[$CuCl_6$]Cl_4 (3-Cl-an = 3-chloroanilinium) indicated a $CuCl_6^{4-}$ complex with two *trans* Cu−Cl bonds significantly shorter than the other four.[1] The **g** tensor of this compound is tetragonal with $g_{\|} \simeq 2.04$ and $g_{\perp} \simeq 2.23$, the symmetry axis being parallel to the short Cu−Cl(3) bonds (Figure 1). Initially, these data were interpreted[1] in terms of a complex with a tetragonally compressed geometry and a d_z^2 ground state, and the significant shift of $g_{\|}$ from the free electron value was explained in terms of a vibronic admixture of $d_{x^2-y^2}$ via a vibration of the form illustrated in Figure 1a. However, a subsequent detailed analysis of the temperature dependence of the **g** tensor and electronic spectrum[2] showed that, at the local level, each complex has an orthorhombically distorted, tetragonally elongated, octahedral geometry (Figure 1b), with the long and intermediate Cu−Cl bonds in dynamic equilibrium. It was suggested[2] that elastic coupling between neighboring complexes probably produces domains of complexes having the long and intermediate bonds aligned in an antiferrodistortive order pattern,[3] although the extent and possible dynamic behavior of these complexes at higher temperatures remain uncertain.

Unfortunately, even at 4 K the EPR (electron paramagnetic resonance) spectra of the individual complexes could not be resolved, because intermolecular electron exchange is faster than the EPR time scale. However, EXAFS measurements at 10 K revealed that a static disorder is present at low temperatures

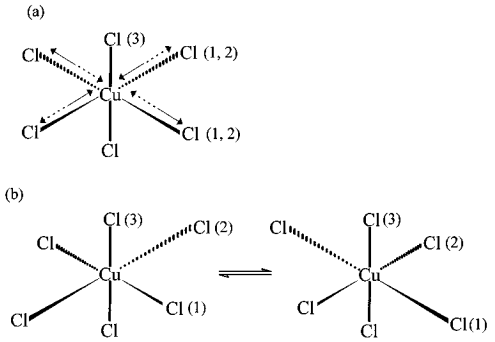

Figure 1. Geometry of the $CuCl_6^{4-}$ polyhedra in (3-Cl-an)$_8$($CdCl_6$)-Cl_4—alternative hypotheses: (a) tetragonally compressed octahedra, perturbed by vibronic coupling. The motions of the Cl^- ligands in the crystallographic (100) plane are illustrated by two types of arrows. (b) The two alternative elongated geometries.

with local Cu−Cl spacings of 2.28(1) Å (2x) parallel to [100] and 2.38(2) (2x) and 2.83(5) Å (2x),[4] in perfect agreement with the estimations from the vibronic coupling model based on the EPR results.[2] The 293 K X-ray structure determination[1] yields compressed $CuCl_6$ octahedra with bond lengths of 2.28 (2x) and 2.61 Å (4x), representing an averaged geometry according to the dynamic or static disorder alternatives illustrated in Figure 1. The underlying elongated geometry, as calculated from the ellipsoids of the thermal motions of the equatorial Cl^- ligands and Cu^{2+} in the (100) plane,[2] again matches nicely with the Cu−Cl spacings derived from EXAFS spectroscopy[4] and the vibronic coupling model.[2]

Although very recently[5] the structural determinations were extended down to temperatures as low as 156 K, no evidence for structural changes was obtained. The space group, unit cell dimensions, and Cu−Cl bond lengths calculated on the basis

* Authors to whom correspondence should be addressed.
† University of Marburg.
‡ University of Tasmania.
⊗ Abstract published in *Advance ACS Abstracts,* May 15, 1996.

(1) Tucker, D.; White, P. S.; Trojan, K. L.; Kirk, M. L.; Hatfield, W. E. *Inorg. Chem.* **1991**, *30*, 823.
(2) Stratemeier, H.; Wagner, B.; Krausz, E. R.; Linder, R.; Schmidtke, H. H.; Pebler, J.; Hatfield, W. E.; ter Haar, L.; Reinen, D.; Hitchman, M. A. *Inorg. Chem.* **1994**, *33*, 2320.
(3) Reinen, D.; Friebel, C. *Struct. Bond.* **1979**, *37*, 1.
(4) Ellis, P. J.; Freeman, H. C.; Hitchman, M. A.; Reinen, D.; Wagner, B. *Inorg. Chem.* **1994**, *33*, 1249.
(5) Wei, M.; Willett, R. D. *Inorg. Chem.*, in press.

S0020-1669(95)01418-2 CCC: $12.00 © 1996 American Chemical Society

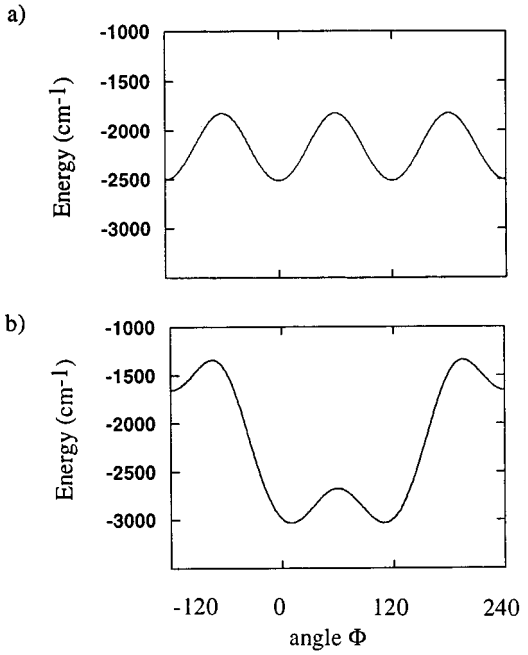

Figure 2. Warping structure of the ground state potential surface of the $CuCl_6^{4-}$ polyhedron in mixed crystals $(3\text{-Cl-an})_8(Cd_{1-x}Cu_xCl_6)Cl_4$ along the angular distortion coordinate ϕ. (a) represents the situation for an initial O_h symmetry, and (b) is if an additional strain corresponding to a compression along the molecular *y* axis (see Figure 3) is present. The parameters of the underlying calculation are specified in The Ground State Potential Surface of the Results and Discussion.

of a static disorder model did not change compared to the results obtained at 293 K, aside from the expected small shrinkage effects caused by the lowering of temperature. Hence, the static disorder—if present—is expected to be of the short-range type, because superstructure reflections are not observed.

The geometric situation as depicted in Figure 1 is explained as originating from the interplay between the tendency of Cu^{2+} to create a tetragonally elongated octahedral geometry (higher order vibronic Jahn−Teller coupling) and a host lattice-induced strain acting as a tetragonal compression along the crystallographic [100] direction.[2] The corresponding vibronic coupling model is illustrated in Figure 2 and will be discussed in greater detail in the following. That the presence of a strain with the sign of a compression is characteristic for this type of structure is documented by the geometry of the $NiCl_6$ polyhedron in the corresponding Ni^{2+} compound, where Ni−Cl bond lengths of 2.38 Å (2*x*) parallel to [100] and 2.49 Å (4*x*) are reported.[6] This distortion must indeed be host site-specific because the electronic ground state of Ni^{2+} in O_h symmetry, $^3A_{2g}$, is nondegenerate and, hence, vibronically stable.

It seemed worthwhile to us to diamagnetically dilute Cu^{2+} in the octahedral position to prevent exchange interactions between the metallic centers and, hence, the averaging of the **g**-tensor components. Not only does this discriminate between the two alternative models in Figure 1, but the temperature dependence of the EPR spectrum should also provide information on the dynamics of the equilibrium between the structural forms. Although we were not able to synthesize the corresponding Zn^{2+} compound where Zn^{2+} possesses an ionic radius similar to that of Cu^{2+},[6] we succeeded in preparing the analogous Cd^{2+} compound and the complete mixed crystal series with the Cu^{2+} complex as both powders and single crystals. The X-ray structure investigation yielded similar unit cell parameters and the same space group for the Cd^{2+} and Cu^{2+} compounds. In particular, EPR measurements with variable Cu^{2+} concentrations and temperatures have been performed to elucidate the bonding properties and the geometry of the $CuCl_6$ polyhedra in the host complex.

Experimental Section

Preparation. The complete mixed crystal series $(3\text{-Cl-an})_8[Cd_{1-x}Cu_xCl_6]Cl_4$ could be synthesized by following preparation methods described in the literature.[1] Apparently the Cd^{2+} and Cu^{2+} compounds possess similar solubilities in water, because the analyses of the crystallized products yield nearly the same Cu^{2+} to Cd^{2+} ratio as that in solution. Typical analytical results are as follows [calculated values for the solution composition (molar %) in parentheses]: N, 7.39 (7.54), C, 38.71 (38.80), H, 3.40 (3.80), Cl, 42.83 (42.95), Cu, 1.02 (0.86), and Cd, 6.47 (6.05) for $x = 0.2$; N, 7.55 (7.62), C, 38.89 (39.19), H, 3.82 (3.84), Cl, 43.10 (43.38), Cu, 2.22 (2.16), and Cd, 4.27 (3.82) for $x = 0.5$. The compounds crystallized as transparent needles with the needle axis parallel to the crystallographic *a* direction.

EPR and Optical Spectroscopy. EPR spectra between 3.7 and 293 K were measured with a Bruker ESP-300 spectrometer at X- and Q-band frequencies, using an Oxford Instruments flow cryostat. A newly developed accessory also allowed the collection of powder data continuously with the temperature at Q band (Bruker ER 5106 QT).

Electronic reflection spectra were recorded against sintered MgO by using a Zeiss PMQII spectrometer, with a Zeiss-Leybold low-temperature attachment.[7] Reflectance data were transformed into log *k*/*s* values according to the theory of Kubelka and Munk.[8]

Structural Investigation. The intensities were collected for a yellow needlelike crystal (0.06 × 0.1 × 0.25 mm) at 20 °C by using a Siemens P4 diffractometer with graphite-monochromated Mo Kα radiation (λ = 0.710 73 Å) by the ω-scan technique in the θ range of $0 < 2\theta \leq 56°$. A total of 3996 independent reflections ($R_{int} = 0.00$) was collected in the index ranges $h = -9$ to -1, $k = -15$ to 14, and $l = -15$ to 14, of which 2597 were considered as observed [$I > 2\sigma(I)$]. Three standard reflections were monitored after every 97 scans to standardize the intensities. The cell parameters were obtained from 22 reflections (θ = 95−25°). Siemens XSCAN was used for data reduction and no absorption correction was applied. The structure was solved in the space group $P\bar{1}$ (No. 2) by three-dimensional Patterson analysis with successive difference Fourier syntheses and by full matrix least-squares refinement on F^2, with anisotropic thermal parameters assigned to all non-hydrogen atoms. The hydrogen atoms were included at their calculated positions with a fixed isotropic thermal parameter (U_{iso} = 0.08). The extinction correction was zero for this structure. The atomic scattering factors were taken from the International Tables.[9]

The final residual value for the conventional $R_1(F) = \sum||F_o| - |F_c||/\sum|F_o|$ is 0.0448. The function $w(F_o^2 - F_c^2)^2$ was minimized with a weighting scheme of the form $w = 1/[\sigma^2(F_o^2) + (aP)^2 + bP]$, with a = 0.0554, $b = 0.00$, and $P = (F_o^2 + 2F_c^2)/3$, resulting in $wR_2(F^2)$ = 0.1111 and a goodness-of-fit GOF(F^2) = 0.857. The final electron density difference synthesis showed no peaks larger than 0.520 or smaller than −0.764 e/Å^3. The crystallographic calculations were carried out on a DEC AXP 3000/300 Workstation with SHELXTL-Plus[10] for the structure solution and molecular graphics. SHELXL 93 was used for the refinement.[11]

The positional and isotropic thermal parameters for the atoms constituting the $CdCl_6^{4-}$ polyhedron in $(3\text{-Cl-an})_8(CdCl_6)Cl_4$ are collected in Table 2. Bond lengths and bond angles for the same polyhedron are found in Table 3. A full listing of data collection parameters, positional and thermal parameters, and bond distances and bond angles is available as supporting information.

Figure 3 shows the unit cell in stereographic projection and the ORTEP illustration of the $CdCl_6^{4-}$ polyhedron. In contrast to the situation for the analogous Cu^{2+} compound,[5] the ellipsoids of the

(6) Shannon, R. D.; Prewitt, C. T. *Acta Crystallogr*. **1969**, *B25*, 925.
(7) Grefer, J.; Reinen, D. Z. *Naturforsch*. **1973**, *28a*, 464.
(8) See Kortüm, G. *Angew. Chem*. **1955**, *67*, 694.
(9) International Tables. *Crystallography C*, **1992**.
(10) Sheldrick, G. M. *SHELXTL-Plus, Release 4.2*; Siemens Analyt. Instruments Inc.: Madison, WI 1990.
(11) Sheldrick, G. M. *Program for the Refinement of Crystal*; University of Göttingen: Göttingen, Germany, 1993.

Table 1. Crystallographic Data for (3-Cl-an)$_8$($CdCl_6$)Cl_4

chemical formula	$C_{48}H_{56}CdCl_{18}N_8$	formula weight (g/mol)	1495.51
a (Å)	8.701(2)	space group	$P\bar{1}$
b (Å)	13.975(2)	T (°C)	20
c (Å)	14.173(2)	λ (Å)	0.7107
α (deg)	81.62(1)	ρ_{calc} (g/cm^3)	1.550
β (deg)	72.92(1)	μ (cm^{-1})	11.31
γ (deg)	77.57(1)	refinement	F^2
V (Å^3)	1603(1)	$R_1(F)^a$	0.0448
Z	1	w$R_2(F^2)^a$	0.1111

[a] $R_1 = \sum||F_o| - |F_c||/\sum|F_o|$; $wR_2 = [\sum\{w(F_o^2 - F_c^2)^2\}/\sum(wF_o^2)^2]^{0.5}$, with $w = 1/[\sigma^2(F_o^2) + (aP)^2 + bP]$ and $P = (F_o^2 + 2F_c^2)/3$.

Table 2. Positional Parameters and Equivalent Isotropic Temperature Parameters (Å^2) of the $CdCl_6$ Polyhedron in (3-Cl-an)$_8$[$CdCl_6$]Cl_4

atom	x	y	z	U(eq)[a]
Cd(1)	0	0	0	0.0333(2)
Cl(1)	−0.0703(2)	−0.0678(1)	0.1915(1)	0.0413(4)
Cl(2)	0.0786(2)	−0.1864(1)	−0.0477(1)	0.0400(4)
Cl(3)	0.2902(2)	−0.0023(1)	0.0019(1)	0.0343(4)

[a] U(eq) is defined as one-third of the trace of the orthogonalized $\mathbf{U}_{ij}$ tensor.

Table 3. Bond Lengths (Å) and Bond Angles (deg) for the $CdCl_6^{4-}$ Polyhedron in (3-Cl-an)$_8$($CdCl_6$)Cl_4[a]

Cd(1)−Cl(3)	2.526(1)	Cl(3)−Cd(1)−Cl(1)	89.66(4)
Cd(1)−Cl(1)	2.676(2)	Cl(3)−Cd(1)−Cl(2)	91.11(4)
Cd(1)−Cl(2)	2.680(2)	Cl(1)−Cd(1)−Cl(2)	88.82(5)

[a] The Cd^{2+} position is centrosymmetric.

thermal motions of the equatorial Cl(1) and Cl(2) ligands along the molecular x and z axes are not significantly different from that of the axial Cl(3) atom (approximately parallel to a), indicating the absence of anomalous disorder or vibronic effects. The $CdCl_6^{4-}$ entity is tetragonally compressed in an even more pronounced way than the $NiCl_6$ octahedron in the analogous nickel compound—presumably due to the larger polarizability of Cd^{2+} compared to Ni^{2+}—again documenting the presence of a distinct host site strain in this type of compound.

Results and Discussion

Cu^{2+}-Doped Mixed Crystals. The $CdCl_6$ octahedra are tetragonally compressed, apparently with a tiny orthorhombic distortion component superimposed, with Cl−Cd−Cl bond angles rectangular within ±1.4° (Table 3). The radial distortion parameter ρ (eq 1) is ≃0.17$_5$ Å for the $CdCl_6$ host polyhedron, where the δa_i values ($i = x, y, z$) are the deviations from the average octahedral spacing of 2.63 Å, which is somewhat larger than the value for the $NiCl_6$ entity in the analogous nickel compound ($\rho = 0.12_5$ Å).

$$\rho = \{2(\delta a_x^{\,2} + \delta a_y^{\,2} + \delta a_z^{\,2})\}^{1/2} \qquad (1)$$

If Cu^{2+} is doped into the Cd^{2+} position in low concentrations, EPR spectra as depicted in Figure 4 are observed. At temperatures above 70 K and at X-band frequency, a spectrum with g values of $g_{\perp'} \simeq 2.20$ and $g_{\parallel'} \simeq 2.03_5$ is observed with a well-resolved copper hyperfine splitting in $g_{\perp'}$ and a $g_{\parallel'}$ signal that is split into 13 components, suggesting participation of the chlorine nuclei (see the analysis to follow and Table 4). The signal shape is that of an axially symmetric **g** tensor, with $g_{\perp'} > g_{\parallel'} > g_0$. The Q-band spectrum, which is more sensitive to **g**-tensor anisotropies than resolving hyperfine splittings, reveals a tiny orthorhombic symmetry component ($g_{z'} \simeq 2.21$, $g_{x'} \simeq 2.20$, $g_{y'} = 2.03$; Figure 4). Below 70 K, a discontinuous change to a spectrum with g values that are typical for a tetragonally elongated octahedron (eq 2, with $\phi \simeq 0°$) occurs, though the

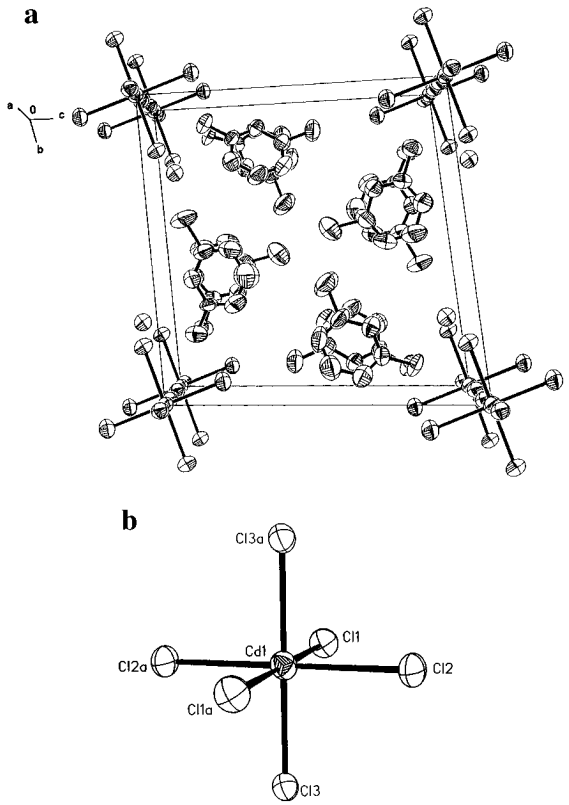

Figure 3. ORTEP drawings of (a) the unit cell of (3-Cl-an)$_8$($CdCl_6$)Cl_4 and (b) the $CdCl_6$ polyhedron. The Cd−Cl(3) distances (molecular y axis) are oriented parallel to the crystallographic a direction, while the Cd−Cl(1) and Cd−Cl(2) spacings (molecular x and z axes) have orientations near the crystallographic c and b directions, respectively.

$g_\perp$ signal is again split by an orthorhombic symmetry component, which is very distinct this time.

$$g_x = g_0 + 4u_x - 2u_x(\cos\phi - \sqrt{3}\sin\phi)$$

$$g_y = g_0 + 4u_y - 2u_y(\cos\phi + \sqrt{3}\sin\phi) \qquad (2)$$

$$g_z = g_0 + 4u_z(1 + \cos\phi)$$

Though most polyhedra have transformed from the geometry characterized by $g_{\parallel'} < g_{\perp'}$ to one corresponding to a tetragonal elongation at ≃55 K, as we conclude from the temperature dependence of some mixed crystals with different Cu^{2+} concentrations, a minor fraction seems to remain in the former state even at 4 K, as is readily deduced from the respective Q-band spectrum (Figure 4). The derived g values are $g_y = 2.04$, $g_x = 2.09$, and $g_z = 2.30$. Equation 2 gives the general expressions for the **g**-tensor components in D_{2h} ligand fields, with the angular distortion parameter ϕ specifying the respective geometries, including those with D_{4h} symmetry (Figure 2). $\phi = 0°$ (120°) corresponds to an elongation along the molecular z (x) direction, $\phi = 60°$ corresponds to a compression along y, and ϕ angles between these limiting values correspond to intermediate D_{2h} geometries.

One can interpret the EPR results on the basis of the ground state potential surface along the angular ϕ coordinate in Figure 2 as follows. Without a strain influence, higher order vibronic Jahn−Teller coupling stabilizes ϕ values of 0°, 120°, and 240°, corresponding to elongated octahedra with $d_{x^2-y^2}$, $d_{y^2-z^2}$, and $d_{z^2-x^2}$ ground states, respectively.[10] A strain in the y direction, with the sign of compression, reduces the saddle-point energy at $\phi = 60°$, giving rise to the potential energy diagram in Figure

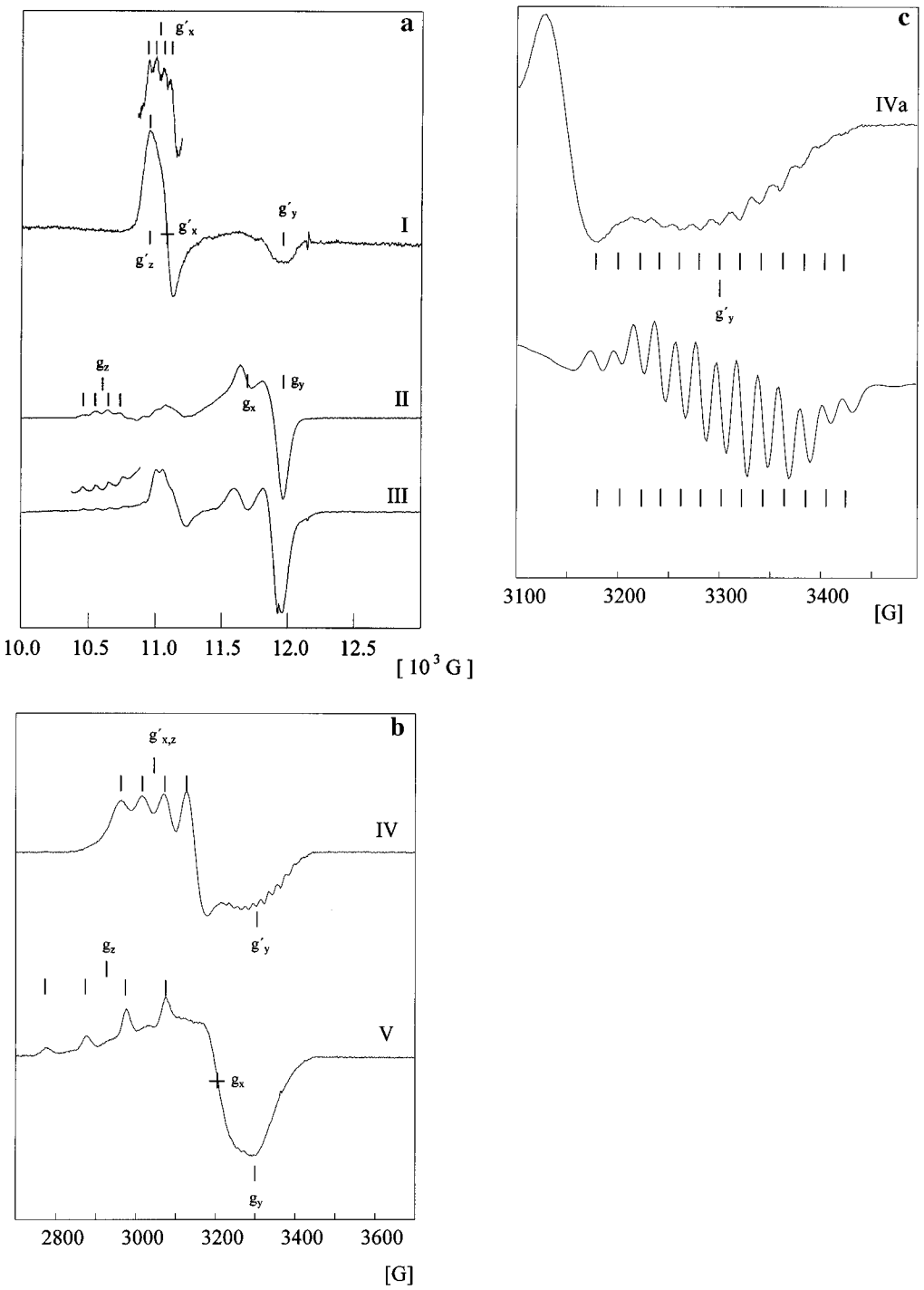

Figure 4. Q-band (a) and X-band EPR spectra (b, c) of Cu^{2+}-doped (3-Cl-an)$_8$($CdCl_6$)Cl_4: I, 293 K (the fine structure from the 100 K spectrum is also shown), 5 mol %; II, 4 K, 10 mol %; III, 4 K, 30 mol % (the A_z hyperfine structure is also shown on a larger scale); IV, 130 K, 1 mol %; V, 4 K, 5 mol %. The overlapping Cl^- and Cu^{2+} hyperfine structure in the $g_{y'}$ signal of IV is shown in an enlarged section (IVa) together with the single-crystal signal observed in the *a* direction.

2b. The minima at $\phi = 0°$ and 120° are energetically stabilized and shifted to slightly higher and lower values, respectively, of the angular coordinate, indicating orthorhombic symmetry contributions. At low temperatures, if only vibronic states within the two lower minima are occupied, octahedra elongated along *z* and *x*—with a superimposed orthorhombic distortion component and an admixture of d_{z^2} and d_{x^2} into the $d_{x^2-y^2}$ and $d_{y^2-z^2}$ ground states, respectively—should be observed (Figure 1b), in perfect agreement with experiment. If upon temperature enhancement vibronic states near or above the saddle point in Figure 2b are thermally occupied, dynamic exchange between the two minima occurs, leading to averaged *g* values with $g_{\perp'} > g_{\parallel'} > g_0$, with the symmetry axis being parallel to the molecular *y* axis. Indeed, a thermal averaging of the low-temperature *g* values according to $g_{\parallel'} \simeq g_y$ and $g_{\perp'} \simeq {}^1/_2(g_x + g_z)$ nicely reproduces the **g′**-tensor components at high temperatures. This geometry may be viewed as being tetragonally compressed within the time scale of the EPR experiment. It reflects purely the strain symmetry, with the Jahn−Teller coupling along the angular ϕ coordinate being dynamically averaged.

The observed orthorhombic symmetry of the **g′** tensor seems to indicate that the host site strain is not purely tetragonal. Indeed, the Cd−Cl(2) bond lengths are slightly larger than the

Table 4. **g** and **A** Hyperfine Tensor Components ($\times 10^{-4}$ cm^{-1}) of (3-Cl-an)$_8$($Cd_{1-x}Cu_xCl_6$)Cl_4 Mixed Crystals[a]

$x < 0.3$	$g_{\|\|'} = 2.03_3$,[b] $g_{\perp'} = 2.19_8$, 2.20_4;[b] $A_{\|\|'} = 2A'[2(Cl3)] = 38.7$,[c] $A_{\perp'} =$ -53, -57[c] (X band, 100 K, values from spectral simulation) (I)
	$g_{y'} = 2.03$, $g_{x'} = 2.20$, $g_{z'} = 2.21$ (Q band, 293 K) (I)
	$g_z = 2.30$,[d] $g_x \approx 2.1$,[d] $g_y \simeq 2.04$;[d] $A_{\|\|} = -107$ (X band, 4−10 K) (II)
	$g_z = 2.30$, $g_x \simeq 2.08$, $g_y \simeq 2.04$; $A_{\|\|} \simeq -107$ (Q band, 4−10 K) (II)
$x > 0.8$	$g_{\|\|}^{ex} = 2.04$, $g_{\perp}^{ex} = 2.19_5$ (X band, 4−293 K)[e]
	$g_{\|\|}^{ex} = 2.03_5$, $g_{\perp}^{ex} = 2.20$ (Q band, 4−293 K)[e]

[a] I, high-temperature spectra; II, low-temperature spectra. [b] Single-crystal values: $g_{y'} = 2.03_5$, $g_{x'} = 2.20$, $g_{z'} = 2.20_5$ (X band, 140 K). [c] At 293 K, $A_{\|\|'}$ is not resolved and $A_{\perp'} \simeq -47$. [d] Single-crystal values: $g_z = 2.30$, $g_x = 2.09$, $g_y = 2.04$ (4 K). [e] Superposition by features as observed for $x < 0.3$.

Cd−Cl(1) spacings (Table 3). Although the difference is within the standard deviations, it also occurs in the nickel compound[5] and, hence, seems to be a real structural effect, which makes ϕ(strain) slightly smaller than 60° and the two minima inequivalent with a tiny energetic preference for the minimum at $\phi >$ 0°. The single-crystal EPR data give evidence that this is indeed the case.

The needle-shaped triclinic crystal was adjusted such that the *ac* or *ab* plane (which could not be distinguished in the habitus) corresponded to the magnetic field plane in the EPR experiment, with the singular needle axis *a* fixed at 0°. Subsequently, the angular dependencies of the EPR signals were measured in the two mutually perpendicular planes. While *a* matches the Cu−Cl(3) direction (molecular *y* axis) to within 2°, the Cu−Cl(2) and Cu−Cl(1) bonds (molecular *z* and *x* axes) deviate from *b** and *c** by less than 10°, where the latter directions correspond to the projections of the *a* and *b* axes into the plane perpendicular to *a* (see Figure 3). The angular dependencies of the **g**-tensor components at 140 K, with $g_{\|\|'}$ oriented parallel to *a*, are shown in Figure 5A. They confirm the EPR powder data and also nicely reveal the tiny orthorhombic strain component (Table 4). The corresponding angular dependencies at 4 K (Figure 5B) reveal the presence of two magnetically inequivalent polyhedra with a perpendicular orientation of the long axes (see Figure 5B caption), corresponding to the geometric situation in Figure 1b, with a copper−copper distance too large to induce exchange coupling. The *g* values again match those derived from the powder spectra (Table 4). It is interesting to note, however, that the intensities of the two signals are significantly different. In certain magnetic field orientations, one signal may even vanish completely. Presumably the stronger intensity spectrum is correlated with the long axis along the Cu−Cl(2) bond, because the host site strain energetically favors this geometry with respect to the polyhedron with an elongation of the Cu−Cl(1) spacing, as already mentioned.

Before the hyperfine structure is analyzed in greater detail, the orthorhombic symmetry component of the $CuCl_6^{4-}$ octahedron at low temperatures is considered more closely. The ligand field spectra of the Cd^{2+}/Cu^{2+} mixed crystals at 293 and 5 K (Figure 6) are very similar to those of (3-Cl-an)$_8$($CuCl_6$)Cl_4, indicating that the geometry of $CuCl_6^{4-}$ polyhedra does not change significantly upon diamagnetic dilution with Cd^{2+}. By adopting the assignment for the Cu^{2+} compound, one obtains (5 K spectra)

$$\begin{aligned} a^2A_g(^2E_g) &\rightarrow b^2A_g(^2E_g): \quad 9000\ cm^{-1} \quad (4E_{JT}) \\ &\rightarrow {}^2B_{1g}(^2T_{2g}): \quad 10\,400\ cm^{-1} \quad (E_z) \\ &\rightarrow {}^2B_{2g}(^2T_{2g}): \quad \simeq 11\,300\ cm^{-1} \quad (E_x) \\ &\rightarrow {}^2B_{3g}(^2T_{2g}): \quad 12\,600\ cm^{-1} \quad (E_y) \end{aligned}$$

Hence, we may use the orthorhombic Cu−Cl bond lengths in (3-Cl-an)$_8$($CuCl_6$)Cl_4 from EXAFS or from the thermal ellipsoids or from the vibronic model (see the Introduction) to interpret the low-temperature *g* values. They correspond to ϕ

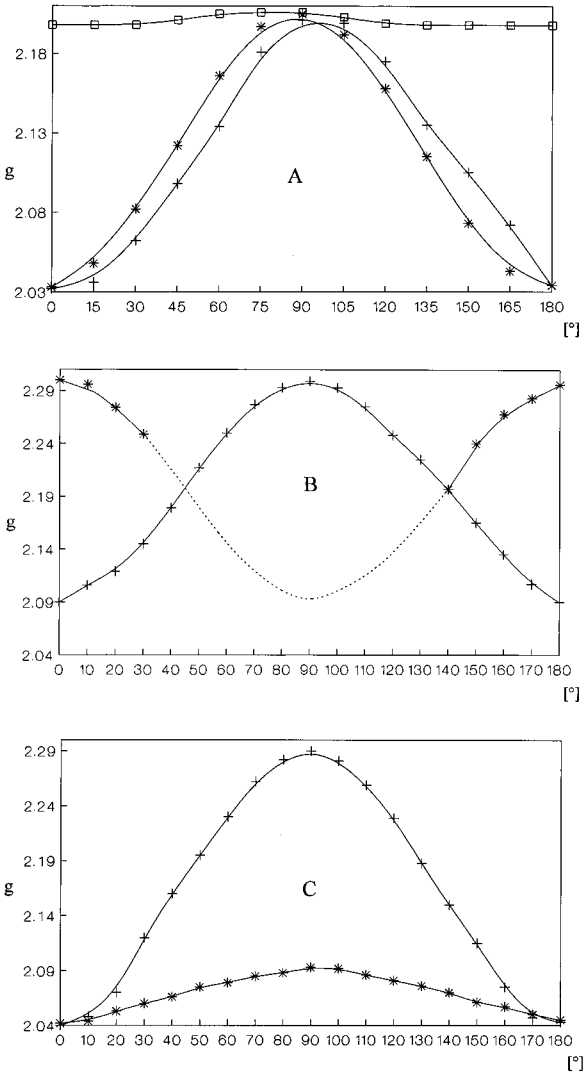

Figure 5. Angular dependencies of the **g**-tensor components for Cu^{2+}-doped (≈10 mol %) (3-Cl-an)$_8$($CdCl_6$)Cl_4 at 140 (A) and 4 K (B, C) (X band). (A) $\theta = 0°$ and 90° refer to the molecular *y* and (approximately) *z* axes for + and *, and the 0° direction for □ is approximately parallel to *x*. (B) $\theta = 0°$ and 90° approximately refer to the molecular *z* (*x*) and *x* (*z*) axes for the two magnetically inequivalent sites * (+). (C) $\theta = 0°$ and 90° are correlated with the molecular *y* and (approximately) *z* (x) directions for the sites + (*). The maximum and minimum positions in the diagrams were shifted to $\theta = 0°$ and 90°. The measured values deviated from these angles by 10−15°, because the molecular *z* and *x* directions are not located in the planes of measurement (see text) on the one hand, and because of experimental single-crystal adjustment uncertainties on the other hand. In the dashed region of (B), the signal intensity nearly vanished in the background and *g* values could not be evaluated.

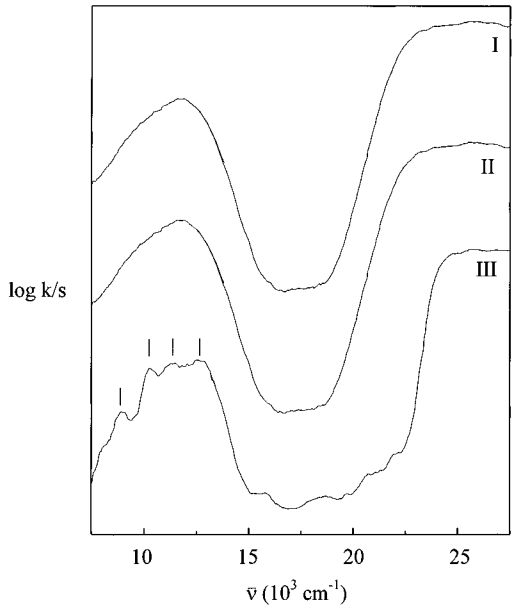

Figure 6. Reflection spectra of mixed crystals (3-Cl-an)$_8$-($Cd_{1-x}Cu_xCl_6$)Cl_4: I, $x = 0.05$, 293 K; II, $x \simeq 0.5$, 293 K; III, $x = 0.5$, 5 K. The marked d−d transitions of spectrum III are specified in the text. The sharp features at 7600 cm^{-1} and below 7500 cm^{-1} are due to the extended cationic frame of the compound.

$\simeq 9(1)°$, as is deduced from eq 3.[12] With this value and the

$$\phi = \arctan\{(\delta a_x - \delta a_y)/\sqrt{3}\delta a_z\} \quad (3)$$

experimental **g**-tensor components, the orbital contributions in eq 2 can be calculated, which are correlated with the covalency factors k_j ($j = x, y, z$) by eq 4, where $\zeta_0 = 830$ cm^{-1} is the free ion spin−orbit coupling constant for Cu^{2+} and the E_j are the preceding ligand field transition energies. Comparatively low

$$u_j = k_j^2\zeta_0/E_j \quad (j = x, y, z) \quad (4)$$

values of $k_z \simeq k_x \simeq 0.69$ and $k_y \simeq 0.64$ result, suggesting rather covalent Cu−Cl bonds. With the help of the estimated value of the angular distortion parameter $\phi = 9°$, the hyperfine splittings in the EPR signals can be analyzed with respect to the properties of the Cu−Cl bond. In the respective eqs 5,[13] the δg_i are the deviations from the spin-only value, and the calibrating factor P is of the magnitude 0.036 cm^{-1} for Cu^{2+}.

$$A_z = P\{(-\kappa - {}^4/_7\cos\phi)\alpha^2 + \delta g_x/14(3 - 2\sqrt{3}\sin\phi)/(2\cos\phi - 1) + \delta g_y/14(3 + 2\sqrt{3}\sin\phi)/(2\cos\phi - 1) + \delta g_z\} \quad (5)$$

$$\phi = 0: \quad A_{\parallel} = P\{(-\kappa - {}^4/_7)\alpha^2 + {}^3/_7\delta g_{\perp} + \delta g_{\parallel}\}$$
$$A_{\perp} = P\{(-\kappa + {}^2/_7)\alpha^2 + {}^{11}/_{14}\delta g_{\perp}\} \quad (5a)$$

$$\Psi_{\mathbf{g}} = \alpha d_{x^2-y^2} - \alpha' L_{x^2-y^2}$$

The expressions for A_x and A_y are generated if ϕ is augmented by 240° and 120°, respectively, and the i indices of the δg_i are shifted according to the sequences $x \rightarrow y \rightarrow z$ and $x \rightarrow z \rightarrow y$, respectively. For the special case of an elongated octahedron and a $d_{x^2-y^2}$ ground state, eq 5a results ($\phi = 0$), where α and α' are the mixing coefficients of the metal ion and the LCAO ligand orbitals, respectively, in the ground state MO. The Fermi contact term is $\kappa = 0.43$ for Cu^{2+} in the case of a $d_{x^2-y^2}$ ground state (eq 5), but may decrease if a d_{z^2} contribution is admixed ($\phi > 0$).[14]

With the parameter set $\phi = 9°$, $\alpha = 0.86$, and $\kappa = 0.27$, a consistent account of the observed hyperfine splittings can be given. The experimental A_z value of the low-temperature spectrum (Table 4) is nicely reproduced (-106×10^{-4} cm^{-1}), while A_y and A_x are calculated to have the magnitudes 32 and 8×10^{-4} cm^{-1}, respectively. Both splittings are not resolved in the partly overlapping g_x and g_y signals of the powder spectra (Figure 4), but are partly in the single-crystal spectra. In switching to higher temperatures, a dynamic averaging process according to $A_{x'} \simeq A_{z'} \simeq {}^1/_2(A_x + A_z)$ and $A_{y'} \simeq A_y$ is expected. In good agreement with this model and the 100 K EPR spectra, hyperfine splittings of -50 and 32×10^{-4} cm^{-1} (Table 4) are calculated. One should keep in mind, however, that a description of the transition from the static to the dynamic disorder just by averaging the respective parameters is rather crude. It does not take into account the change in the electronic wave function in the higher vibronic states, which are more strongly delocalized along the angular ϕ coordinate than those localized in either of the two minima (Figure 2).

When the magnetic field is parallel to the short Cd−Cl(3) direction, a pattern of 13 equispaced lines is observed (Figure 4). Such a pattern is expected if the magnitude of the hyperfine coupling with the copper nucleus (spin I(Cu) = $^3/_2$) along this direction is approximately twice that with the nuclear spins of the two equivalent chlorine atoms Cl(3) (spin I(Cl) = $^3/_2$). Here, the splittings due to the other chlorine atoms, and the slight differences in splitting expected for the two isotopes of chlorine, are not resolved. The observed relative intensities of the lines (Figure 4, IVa) nicely reproduce the expected intensity ratios (1:2:4:6:7:8:8:8:7:6:4:2:1). The value of the chlorine superhyperfine coupling constant, $\simeq 19.4 \times 10^{-4}$ cm^{-1} (from spectral simulations), is in good agreement with that reported[15] for the interaction parallel to the metal−chlorine bonds of the planar $CuCl_4^{2-}$ complex in Cu^{2+}-doped K_2PdCl_4 (23×10^{-4} cm^{-1}), when it is remembered that slightly longer Cu−Cl bonds should be present in the six-coordinate complex.

As expected, a chloride hyperfine structure is also observed in the low-temperature single-crystal signals along the molecular x (z) and y directions, connected with the short Cu−Cl spacings. They are only partly resolved, however, and could not be analyzed quantitatively. All other interactions with the ligand nuclei should be smaller and, hence, are not resolved. The Fermi contact term in the proposed parameter set has decreased considerably with respect to the value for a $d_{x^2-y^2}$ or $d_{y^2-z^2}$ ground state and indicates a distinct 4s admixture into the electronic ground state wave function caused by the orthorhombic ligand field component ($\phi = 9°$).[14] The mixing coefficient α—though still in a range valid for a predominantly ionic bond—is smaller than that derived for CuF_6^{4-} polyhedra (>0.9)[12] with the more electronegative fluorine ligand.

The features near the $g_{\perp'}$ positions in the Q-band spectra at 4 K (Figure 4, II and III), whose intensity increases with x ($g_{\perp}^{ex}$), are due to exchange clusters, and the corresponding $g_{\parallel}^{ex}$ signal contributes to the spectral intensity at g_y. These clusters are defined and discussed in the next section. The partly resolved hyperfine structure superimposed on the $g_{\perp'}$ signals indicates that only weakly coupled dimers might also be present in addition to more extended clusters.

(12) Reinen, D.; Atanasov, M. *Magn. Res. Rev.* **1991**, *15*, 167.
(13) Ozarowski, A.; Reinen, D. *Inorg. Chem.* **1985**, *24*, 3860.
(14) Steffen, G.; Reinen, D.; Stratemeier, H.; Riley, M. J.; Hitchman, M. A.; Matthies, H. E.; Recker, K.; Wallrafen, F.; Niklas, J. R. *Inorg. Chem.* **1990**, *29*, 2123.
(15) Chow, C.; Chang, K.; Willett, R. D. *J. Chem. Phys.* **1973**, *59*, 2629.

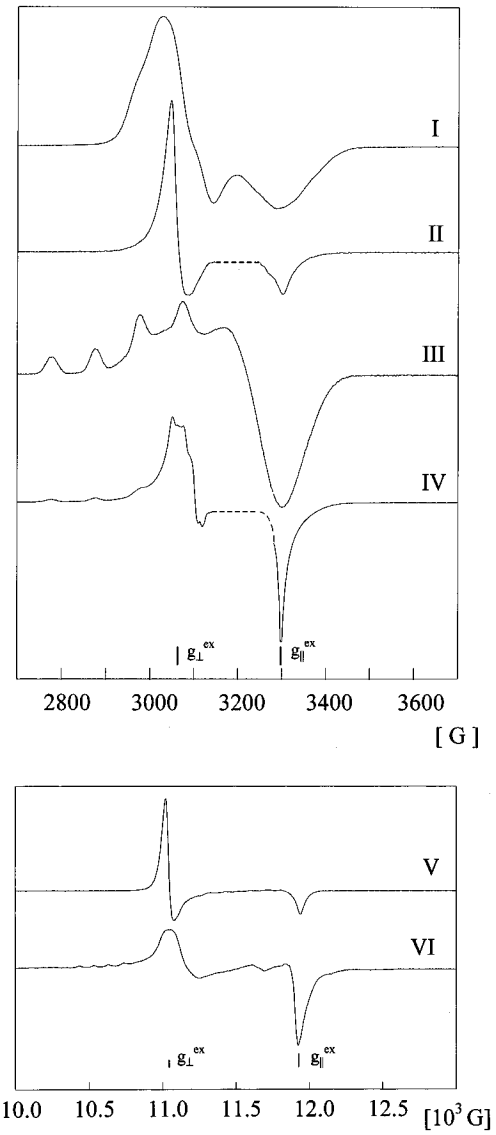

Figure 7. EPR powder spectra of mixed crystals (3-Cl-an)$_8$($Cd_{1-x}Cu_xCl_6$)-Cl_4 for high x values at X band: I and III ($x = 0.6$), 293 and 12 K; II and IV ($x = 0.7$), 293 and 10 K. At Q-band frequencies: V and VI ($x = 0.8$), 293 and 4 K.

Mixed Crystals with High Copper Concentrations. Increasing the Cu^{2+} concentration in the mixed crystals above $x \simeq 0.3$ washes out the hyperfine splittings in the high-temperature spectra by line broadening due to exchange effects between $CuCl_6^{4-}$ neighbors (Figure 7, I). At $x > 0.6$ additional features appear, which correspond to the spectrum characteristic for (3-Cl-an)$_8$($CdCl_6$)Cl_4[1,2] (Figure 7, II and V). We may understand the low-temperature EPR spectra as superpositions of essentially two species: (1) statically elongated octahedra with a distinct orthorhombic symmetry component superimposed and with the long axis extending along the molecular z and/or—slightly less preferred—x directions and (2) exchange-coupled pairs or extended clusters of $CuCl_6^{4-}$ polyhedra possessing a mutually perpendicular orientation of the long axes along the molecular z and x directions (Figure 2b).

For the latter clusters, exchange coupling according to eq 6 is expected,[2] leading to **g**-tensor components of $g_\parallel^{ex} = 2.04$ and $g_\perp^{ex} = 2.19$, which are in good correspondence with those values observed here (Table 4, Figure 7) and for $x = 1.0$.[2] The line

$$g_\parallel^{ex} = g_y \qquad g_\perp^{ex} = {}^1/_2(g_x + g_z) \tag{6}$$

widths of the respective spectra, which show the features typical of exchange narrowing, are consistent with the presence of magnetic interactions in the pure copper(II) compound.[2] At temperatures above ≈55 K dynamical averaging is expected, as we may infer from the EPR results for low doping concentrations (see Results and Discussion, Cu^{2+}-Doped Mixed Crystals). Because dynamic and electronic exchange induces analogous g-averaging effects (eq 6), however, we may distinguish between the two mechanisms only by the line shape. The spectra for $x = 0.7$ in Figure 7 (II and IV) in particular give distinct evidence for the presence of exchange clusters, with a strongly narrowed $g_\parallel^{ex}$ signal at 10 K.

The Ground State Potential Surface. The parameters determining the ground state potential surface of Cu^{2+} on the Cd^{2+} sites in (3-Cl-an)$_8$($CdCl_6$)Cl_4 are readily calculated by utilizing the respective equations,[12] which describe the influence of linear and higher order Jahn−Teller coupling on an octahedral E_g state in the presence of strain. They are valid under the—here fulfilled—condition that the strain is small compared with the linear vibronic coupling. The radial distortion parameter of the $CuCl_6^{4-}$ polyhedra in mixed crystals (3-Cl-an)$_8$($Cd_{1-x}Cu_xCl_6$)-Cl_4, as calculated from the Cu−Cl bond lengths in the Cu^{2+} compound ($x = 1.0$) utilizing eq 1, amounts to $\rho_t = 0.61(2)$ Å, while the strain-induced distortions in the Cd^{2+} host ($x = 0$) and in the corresponding Ni^{2+} compound are $\rho_s = 0.17_5$ and 0.12_5 Å, respectively. The ground state splitting $4E_{JT} \simeq 9000$ cm^{-1} (see ligand field spectra) allows an estimation of the linear vibronic coupling parameter A_1 on the basis of the radial distortion parameter ρ_t found for the $CuCl_6^{4-}$ polyhedron, if a proper choice for the higher order Jahn−Teller coupling terms comprising β is made (eq 7).

$$4E_{JT} \simeq 2A_1\rho_t + 2\beta \cos 3\phi \tag{7}$$

Here 2β is the energy difference between the minima and saddle points in Figure 2a, and we anticipate the value $\beta = 350$ cm^{-1} obtained by using the vibronic coupling model described in the following. With $\phi = 9°$, A_1 is estimated to be $\simeq$6900 cm^{-1} $Å^{-1}$. ρ_t, according to eq 8, is the sum of the Jahn−Teller-induced distortion ρ_{JT} and a strain contribution. With

$$\rho_t \simeq \rho_{JT} + \rho_s \cos(\phi - \phi_s) \tag{8}$$

$\rho_s = 0.12_5$ Å, adopted from the Ni^{2+} compound, and $\phi_s = 60°$ (compression along the molecular y direction), one estimates that the strain part of the total distortion amounts to about 13%. The strain parameter, deduced from eq 9, is about $S = 850$ cm^{-1}, which is somewhat larger in magnitude than the value $S = 600$ cm^{-1} used previously.[2] Finally, one may estimate the ground

$$S = A_1\rho_s \tag{9}$$

state stabilization by the combined action of Jahn−Teller coupling and strain from eq 10.[12] It is approximately 2700 cm^{-1}.

$$E_m = -{}^1/_2A_1\rho_{JT} - \beta \cos 3\phi - S\cos(\phi - \phi_s) \tag{10}$$

The preceding values for A_1 and S may be used as the basis for a vibronic calculation.[2] This requires an estimate of the energy of the Jahn−Teller vibration (details of the relationships between the various parameters are given in ref 16). The force constant is given by eq 11, and substitution of $A_1 = 6900$ cm^{-1} $Å^{-1}$ and $\rho_{JT} = 0.53$ Å yields $k = 13\,000$ cm^{-1} $Å^{-2}$. For a

(16) Riley, M. J.; Hitchman, M. A.; Reinen, D. *Chem. Phys.* **1986**, *102*, 11.

$$k \simeq A_1/\rho_{JT} \tag{11}$$

ligand mass appropriate to chloride, $M = 35.45$ amu, the relationship in eq 12 yields an energy $h\nu \simeq 110$ cm^{-1} for the e_g vibration. Both this energy and the A_1 value (=6900 cm^{-1} Å^{-1}) are distinctly lower than those used in previous studies, namely, ≃150 cm^{-1} [2] and 10 500 cm^{-1} Å^{-1} (estimation from angular overap calculations).[12] While the overall Jahn−Teller distortion of the $CuCl_6^{4-}$ complex is strongly influenced by A_1 and $h\nu$, the warping parameter is expected to be very sensitive to the orthorhombic distortion.[17]

$$h\nu = 5.806\sqrt{k/M} \tag{12}$$

We have carried out vibronic calculations as described previously[2] for a range of β values, and optimum agreement with the observed g values and bond lengths was obtained by using $\beta = 350$ cm^{-1}. This value appears to be more realistic than the previous estimate $\beta = 550$ cm^{-1} [2] and compares well with the values 290 cm^{-1} reported by Bacci for Cu^{2+}-doped NaCl[18] and 300 cm^{-1} for the $Cu(H_2O)_6^{2+}$ ion.[19] The g values and bond lengths for the lowest vibronic state of the $CuCl_6^{4-}$ complex calculated with the parameter set $A_1 = 6900$ cm^{-1} Å^{-1}, $h\nu = 110$ cm^{-1}, and $S = 850$ cm^{-1} are in reasonable agreement with the experimental values (in parentheses): $g_y = 2.03$ (2.04); $g_x = 2.07$ (≈2.09); $g_z = 2.34$ (2.30); Cu−$Cl_y = 2.20$ (2.28) Å; Cu−$Cl_z = 2.38$ (2.38) Å; Cu−$Cl_x = 2.92$ (2.83) Å.

Here, an isotropic orbital reduction coefficient of 0.69 was used in the calculation. We included a very small orthorhombic component of the strain in the calculation (0.3 cm^{-1}), corresponding to a φ_s value deviating slightly from 60° (59.8°). This induces, in agreement with the experimental result, a slightly higher energy of the form in which the g values and bonds along the x and z directions are reversed. The calculated distortion in the absence of Jahn−Teller coupling, $\rho_s = 0.12$ Å, is also in good agreement with that observed for the nickel complex.

The variation in the energy of the complex as a function of ϕ plotted at the Jahn−Teller radius of the lowest minimum, the calculation being based on the preceding parameters, is shown in Figure 2b. A similar plot in the absence of lattice strain is given in Figure 2a. It may be seen that the barrier height between the minima at 10° and 110° is substantial, ≈370 cm^{-1}, so that the two lowest vibronic wave functions are strongly localized in these two wells. The first wave function showing a significant delocalization across the barrier lies 292 cm^{-1} above the ground state.

A test of the self-consistency of this model is provided by the temperature at which the EPR spectrum undergoes a transition from a dynamically averaged signal to one where the observed signals associate with the wave functions, which are localized in the wells at $\varphi = 9°$ and 111°, respectively (Figure 2b). Here, the energy difference between the signals, measured in frequency units, approximately equals the rate of exchange R between the two orientations, as described by the relationship in eq 13.[20] μ_B is the Bohr magneton and h is Planck's constant.

$$R \approx |g_x - g_z|\mu_B \mathbf{B}\pi/\sqrt{2h}) \tag{13}$$

Substitution of $g_x = 2.09$, $g_z = 2.30$, and the average magnetic field of the signals $\mathbf{B} = 0.34$ T into eq 13 yields the rate $R \approx 2.09 \times 10^9$ s^{-1}. Since the energy difference between the structural isomers is small compared with the activation energy ΔE^*, the latter can be estimated from eq 14,[21] where k is the Boltzmann constant and R is the gas constant. Substitution of

$$R \approx kT(\exp[-\Delta E^*/(RT)]/h \tag{14}$$

the preceding exchange rate and the temperature of coalescence $T \approx 60$ K into eq 14 yields $\Delta E^* \approx 260$ cm^{-1}. While this activation energy is not expected to be identical with the energy of the first delocalized wave function, 292 cm^{-1}, it seems reasonable that they are similar in magnitude.

Conclusions

The spectroscopic results on the mixed crystals $(3\text{-an-Cl})_8(Cd_{1-x}Cu_xCl_6)Cl_4$ provide evidence that the geometry and bonding properties of the $CuCl_6^{4-}$ polyhedra in the Cd^{2+} matrix are essentially identical to those for $x = 1.0$. Hence, cooperative elastic and electronic effects seem to be very small, as expected for a situation where the interacting polyhedra are isolated from each other in the lattice.[3,12] On the basis of the temperature-dependent EPR investigation of the doped compounds, one may infer, for $(3\text{-an-Cl})_8(CuCl_6)Cl_4$, that above ≈55 K the $CuCl_6^{4-}$ polyhedra are dynamically exchanging more rapidly than the EPR time scale, while below this temperature the system freezes into statically elongated octahedra with a distinct orthorhombic symmetry component superimposed (Figure 1b), which are elastically and electronically coupled (antiferrodistortive pairs or clusters). The EPR analysis was more successful for isolated $CuCl_6^{4-}$ polyhedra embedded in a diamagnetic matrix than for the copper compound itself, because in the latter case weak dipolar or exchange coupling leads to cooperative g values, which do not allow full characterization of the molecular **g** tensor. It remains to be considered whether the static order in the low-temperature region is short-range or long-range in nature with an antiferrodistortive pattern. In the latter case a superstructure is expected to evolve below ≃55 K. This temperature is lower than those for which X-ray structure analyses are available.[5]

The bonding properties of the $CuCl_6^{4-}$ polyhedra have been characterized by utilizing the spectroscopic results obtained and applying an appropriate vibronic coupling model.[16,19]

Acknowledgment. The authors greatly appreciate the valuable experimental assistence of M. Soeberdt in preparing the mixed crystals and the support of Prof. Dr. W. Massa in the structure determination. They thank the "Deutsche Forschungsgemeinschaft", the Alexander von Humboldt Foundation, and the "Fonds der Chemischen Industrie" for financial support, as well as Dr. H. Stratemeier and Dr. M. J. Riley (Hobart) for useful discussions. They also thank Miss S.-L. Lee (Marburg) for the spectral simulations.

Supporting Information Available: Tables giving positional and isotropic thermal parameters for $(3\text{-chloroanilinium})_8[CdCl_6]Cl_4$ (Table S1), anisotropic thermal parameters for all non-hydrogen atoms (Table S2), and bond distances and angles (hydrogen atoms excluded) (Table S3) are provided in separate and consecutive numbering (7 pages). Ordering information is given on any current masthead page.

IC951418E

(17) Reinen, D.; Krause, S. *Inorg. Chem.* **1981**, *20*, 2750.
(18) Bacci, M. *Chem. Phys.* **1979**, *40*, 237.
(19) Riley, M. J.; Hitchman, M. A.; Wan Mohammed, A. *J. Chem. Phys.* **1987**, *87*, 3766.
(20) Carrington, A.; McLachlan, A. D. *Introduction to Magnetic Resonance*; Harper and Row: New York, 1967; p 207. Note that the frequency ω in this reference is given in radians per second. This may be converted to frequency in hertz (ν) via the relationship, $\omega = 2\pi\nu$.
(21) Laidler, K. J. *Chemical Kinetics*, 3rd ed.; Harper and Row: New York, 1987; p 94.